Biointerface Research in Applied Chemistry
Open-Access Journal (ISSN: 2069-5837)

Article
Volume 16, Issue 1, 2026, 14
https://doi.org/10.33263/BRIAC161.014

In-silico Evaluation of Five Antituberculosis Drug Candidates Targeting Shikimate Kinase of *Mycobacterium tuberculosis*

Nuki Bambang Nugroho [1,*], Fahmi Nurhidayat [2], Annisa Annisa [2,*]

[1] Research Center for Vaccine and Drug, National Agency for Research and Innovation (Badan Riset dan Inovasi Nasional), Cibinong, West Java, Indonesia; nuki001@brin.go.id;
[2] Department of Biology, Faculty of Mathematics and Natural Sciences, Universitas Padjadjaran, Jatinangor, 45363, West Java, Indonesia; fahmi21003@mail.unpad.ac.id (F.N.); annisa2016@unpad.ac.id (A.A.);
* Correspondence: nuki001@brin.go.id (N.B.N.); annisa2016@unpad.ac.id (A.A.);

Received: 18.09.2025; Accepted: 14.01.2026; Published: 15.02.2026

Abstract: The shikimate pathway is considered a promising target for the development of new anti-tuberculosis drugs (ATD) due to its vital role in the survival of *Mycobacterium tuberculosis* and its absence in mammals, which minimizes the risk of toxicity. The present study aimed to identify *Mycobacterium tuberculosis* shikimate kinase (*Mt*SK) inhibitors as anti-tubercular agents from chemical libraries of the Asteraceae and Fabaceae families using molecular docking, pharmacophore evaluation, and ADMET prediction. A molecular docking study using the Molecular Operating Environment (MOE) was employed to screen 5137 compounds from the Asteraceae chemical library and 4653 from the Fabaceae chemical library. This docking study used a rigid docking receptor and an induced-fit receptor technique to simulate interactions between receptors and compounds. The screened compounds were then validated using pharmacophore and ADMET analyses to demonstrate their positive characteristics. The molecular docking simulation identified phenylethyl β-D-glucopyranoside and galacturonic acid as the most promising candidates for targeting MtSK, based on their binding energy scores and the suitability of interacting with key *Mt*SK residues (Asp34, Arg58, Gly80, Arg136). Moreover, this compound also shared pharmacophore features with SKM, complied with Lipinski's and Veber's drug-likeness rules, exhibited drug-likeness properties, and was non-toxic. This work identified five drug-like hit compounds as *Mt*SK inhibitors, promising candidates for the development of a new anti-tuberculosis therapy, and warrants additional experimental investigation. Phenylethyl β-D-glucopyranoside and galacturonic acid are the most promising *Mt*SK inhibitor candidates.

Keywords: *Mycobacterium tuberculosis*; shikimate kinase; molecular docking; Fabaceae; Asteraceae.

1. Introduction

Tuberculosis cases are rising, with 10.8 million infections and 1.25 million deaths in 2024 [1]. Despite declining mortality rates, *Mycobacterium tuberculosis* remains the world's leading infectious cause of death. Drug-resistant strains worsen TB, rendering anti-TB drugs ineffective. In 2022, 410,000 of 10.6 million cases were multidrug-resistant, causing 15–20% of TB deaths. Misuse of anti-TB drugs drives resistance, highlighting the need for new treatment strategies.

Identifying new therapeutic targets is crucial to combat TB resistance. *M. tuberculosis* shikimate kinase (*Mt*SK), an enzyme in the shikimate pathway essential for synthesizing aromatic amino acids, folate, and ubiquinone, is a promising target [2,3]. Inhibiting *Mt*SK disrupts nutrient biosynthesis, which is vital for bacterial survival, and may enhance immune killing through nutrient stress [4]. As *Mt*SK exists only in plants and microbes, targeting it could minimize human toxicity [5].

The shikimate pathway, found in plants, microbes, and some parasites but absent in animals, produces chorismate, a precursor of aromatic amino acids. All organisms using this pathway follow seven enzymatic steps, with shikimate kinase (SK) catalyzing the fifth step by phosphorylating shikimate to form shikimate-3-phosphate (S3P). Crystal structures of microbial SKs from *M. tuberculosis*, *E. chrysanthemi*, *E. coli*, and *H. pylori* have been resolved, guiding inhibitor research focused primarily on microbial targets such as *Mt*SK. Due to microbial resistance, novel inhibitors with distinct action sites are sought. Compounds such as ilimaquinone, 6-cyclohexamidomanzamine A, and Rottlerin have shown effective *Mt*SK inhibition. Bioinformatics and compound libraries support the discovery of anti-tuberculosis agents, including potent analogs like *N*, *N*-di(3-bromo-1*H*-indol-5-ylmethyl)amine (Ki = 8.2 µM for *Mt*SK) and *N*, *N*-di(naphth-2-ylmethyl)amine (Ki = 300 nM for *Hp*SK). Extracts from *Sutherlandia frutescens* and synthesized 7-chloroquinoline derivatives also exhibit strong antituberculosis activity [3].

Phytochemical compounds from medicinal plants show great potential as natural inhibitors for tuberculosis (TB) treatment [6]. Ethnopharmacological studies have identified several plants traditionally used against TB, including *Abrus precatorius*, *Pongamia pinnata*, and *Camchaya calcarea* [7-10]. Empirical evidence supporting these uses has led researchers to focus on species from the Asteraceae and Fabaceae families as sources of potential TB drug candidates. Community knowledge plays a key role in selecting safe, non-toxic plants for further evaluation [11].

This study employs in silico molecular docking to screen chemical compounds for potential new therapeutics. This method addresses the limitations of ethnopharmacological research, which often lacks molecular-level explanations for the activity of plant extracts. It complements existing in vitro studies by identifying specific compounds responsible for antibacterial effects [10, 12,13].

In molecular docking screening, compounds were selected as drug candidates based on binding energy and interactions with key *Mt*SK residues (Asp34, Gly80, Arg136), compared with SKM as the native ligand in *Mt*SK. Hit compounds with stronger binding energy than SKM and have interactions with key *Mt*SK residues predicted to bind with SKM as MtSK substrate in its site competitively. Thus, the hit compounds can inhibit the catalysis of SKM to shikimate-3-phosphate. After that, the hit compounds from molecular docking were selected again based on pharmacophore similarity to SKM, compliance with Lipinski's and Veber's rules, favorable drug-likeness, and acute toxicity.

This study aims to identify phytochemical compounds from the Asteraceae and Fabaceae families with potential *Mt*SK inhibitory activity and to analyze their molecular interactions with target receptors. From five drug-like hits, two promising *Mt*SK inhibitors were identified. The findings offer insight into phytochemical-based anti-TB candidates and their inhibition mechanisms, as revealed by binding energy, interaction types, and the amino acid residues involved.

2. Materials and Methods

This investigation adopts a comprehensive methodological framework encompassing the acquisition and refinement of protein structural data and phytochemical compound libraries. Subsequent stages involve the identification of prospective *Mycobacterium tuberculosis* shikimate kinase (*Mt*SK) inhibitors via molecular docking and pharmacophore-based screening techniques. Additionally, the pharmacokinetic and toxicity profiles of candidate compounds are evaluated through ADMET (Absorption, Distribution, Metabolism, Excretion, and Toxicity) predictions, as depicted in the accompanying Figure 1.

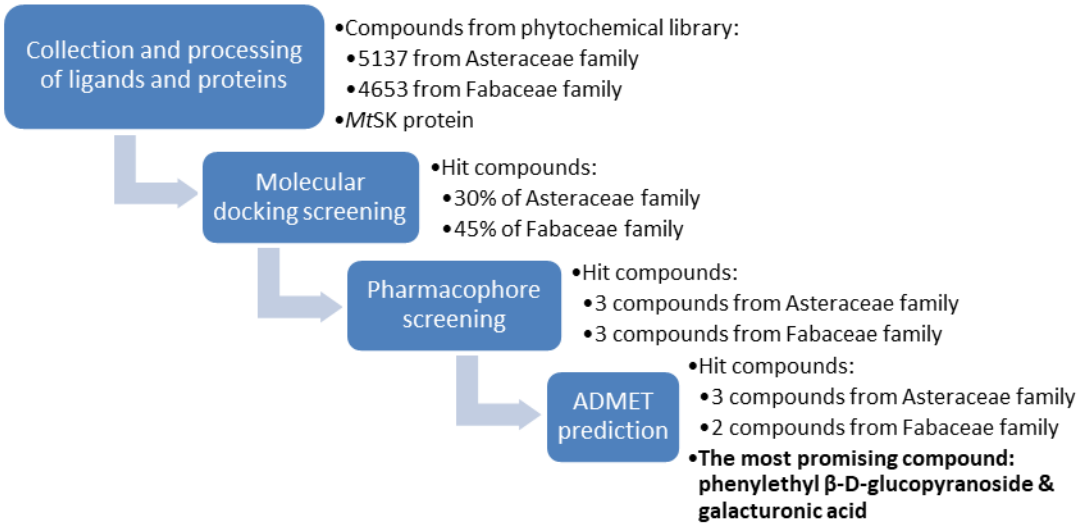

Figure 1. The study methodology.

2.1. Hardware, software, and websites.

Computational analyses were conducted on a Lenovo workstation operating on Windows 11 Pro, equipped with an Intel Core i7-10700K processor (base and turbo frequencies of 3.70 GHz and 3.80 GHz, respectively), an NVIDIA Quadro P1000 GPU, integrated Intel UHD Graphics 630, and 64 GB of RAM. The primary software platforms utilized included Molecular Operating Environment version 2022.02 (MOE 2022.02) and ChemDraw version 21.0.0. Online resources employed for compound retrieval, decoy generation, and pharmacokinetic and toxicity prediction comprised the Lotus Database (https://lotus.naturalproducts.net/), LiDEB decoy generator (https://lideb-lude-2.streamlit.app/), SwissADME (http://www.swissadme.ch/), and ProTox 3.0 (https://tox.charite.de/protox3/).

2.2. Ligands and proteins.

This study's materials included a library of plant chemical compounds from the Asteraceae and Fabaceae families, as well as positive and negative control chemicals (decoys) and 3D protein structures.

Phytochemical compound libraries were obtained in Structure Data File (SDF) format from the Lotus Database (https://lotus.naturalproducts.net/). Selection of plant species was guided by documented ethnopharmacological evidence supporting their traditional use in the treatment of tuberculosis or related symptomatic conditions, as well as their representation within the database. The overall number of plant taxa incorporated and the corresponding count of retrieved chemical constituents are summarized in Table 1.

Table 1. Number of plants and compounds from the chemical library.

Family	Number of species	Number of compounds
Asteraceae	62	5137
Fabaceae	68	4653

A total of 15 positive control compounds, identified as inhibitors of *Mt*SK, were selected based on previously reported literature (Table 2). These reference compounds were either obtained from the PubChem database in 2D SDF format or manually constructed in ChemDraw and subsequently saved in the same format. Positive controls were characterized by experimentally validated inhibitory activity against MtSK, as demonstrated in both in vitro and in vivo assays reported in the literature (Table 2).

Table 2. Positive controls.

Positive control	Literature
(1R,6S,10S)-6,10-Dihydroxy-4-propyl -2-oxabicyclo[4.3.1] deca-4(*Z*),7-diene-8-carboxylic acid	[14]
(1R,6S,10S)-4-Ethoxymethyl-6,10-dihydroxy-2-oxabicyclo[4.3.1] deca-4(*Z*),7-diene-8-carboxylic acid	[14]
(1R,6S,10S)-4-Benzyloxymethyl-6,10-dihydroxy-2-oxabicyclo[4.3.1] deca-4(*Z*),7-diene-8-carboxylic acid	[14]
(1R,6S,10S)-4-Hydroxylmethyl-6,10-dihydroxy-2-oxabicyclo[4.3.1] deca-4(*Z*),7-diene-8-carboxylic acid	[14]
(1R,4S,6S,10S)-6,10-dihydroxy-4-methyl-2-oxabicyclo[4.3.1] dec-7-ene-8-carboxylic acid	[14]
(1R,4R,6S,10S)-6,10-dihydroxy-4-methyl-2-oxabicyclo[4.3.1] dec-7-ene-8-carboxylic acid	[14]
Linoleic acid (CID 5280934)	[15]
Ilimaquinone (CID 72291)	[16]
Rottlerin (CID 5281847)	[17]
Zinc15707201 (ethyl 4-[[(6S)-6-(3-propan-2-yl-1,2,4-oxadiazol-5-yl)-3,4,6,7-tetrahydroimidazo[4,5-c]pyridine-5-carbonyl]amino]benzoate) (CID 26761883)	[18]
Zinc20462780 (CID 28959381)	[18]
Zinc15707234 (CID 26761912)	[18]
Zinc15675581 (CID 26744826)	[18]
Zinc15707188 (ethyl 4-[[(6S)-6-[3-(4-chlorophenyl)-1,2,4-oxadiazol-5-yl] -3,4,6,7-tetrahydroimidazo[4,5-c] pyridine-5-carbonyl]amino]benzoate) (CID 26761872)	[18]
Zinc20464408 (CID 28961011)	[18]

Negative control compounds, referred to as decoys, were defined by their minimal or absent binding affinity in comparison to the reference ligand. These decoys were generated using the LiDEB decoy generator (https://lideb-lude-2.streamlit.app/), which produces structurally dissimilar molecules presumed to exhibit poor interaction with the target protein due to steric or physicochemical incompatibilities. Although not experimentally validated against the molecular target, such compounds are computationally predicted to lack significant binding potential. LiDEB outputs decoys in Simplified Molecular Input Line Entry System (SMILES) format, which are subsequently rendered in ChemDraw and saved in the two-dimensional Structure Data File (2D SDF) format. A total of 163 decoy compounds were employed in this study.

The three-dimensional structure of *Mt*SK was retrieved from the Protein Data Bank (https://www.rcsb.org). Protein models selected for analysis were required to possess high crystallographic resolution (less than 2 Å) and exhibit no reported mutations, as detailed in Table 3. The active site was delineated based on the interaction interface between *Mt*SK and its co-crystallized ligand, shikimate (SKM).

Table 3. *Mt*SK protein.

Code	Identity	Ligand	Protein type	Resolution	Mutation
2IYQ	*Mycobacterium tuberculosis* Shikimate Kinase	SKM [1] ADP [2] TRS [3]	Transferase	1.8 Å	No

[1] Shikimic acid; [2] Adenosine diphosphate; [3] Tris buffer.

2.3. Protein preparation.

The downloaded three-dimensional protein structure in PDB format is then generated using the MOE 2022.02 application's QuickPrep menu with the default parameters. The default QuickPrep feature calibrates the protein structure using a variety of processes, including protonation, partial-charge calculation, hydrogen-atom addition, water-molecule removal, protein structure refinement, and ligand and binding-pocket energy minimization. After the protein is prepared, the Tris buffer (TRS) and ADP molecules are separated from the protein, leaving only the *Mt*SK protein complex and the SKM ligand.

2.4. Preparation of test ligand, positive control, and decoy.

The compounds to be prepared need to be entered into a database and saved in the MOE 2022.02 database (mdb) format. Compound preparation is carried out using the MOE 2022.02 application's Wash feature. The Wash feature panel in the MOE is opened with the database command DBV>Compute>Molecule>Wash. The Wash function parameters consisted of choosing the dominant protonation state at pH 7 and rebuilding the 3D coordinates while preserving the existing chirality. The Wash application can be used to correct errors across an entire database of structures, such as alkali-metal-oxygen single bonds, protonated strong acids, deprotonated strong bases, badly scaled bond lengths, and explicit counter-ion structures. Compound preparation produces a database comprising 3D representations of the final compounds.

2.5. Molecular docking.

Docking validation involves re-docking the SKM ligand to *Mt*SK to assess RMSD, and docking control compounds to evaluate the system's ability to distinguish inhibitors from decoys based on affinity energy. Potential *Mt*SK inhibitors are identified through compound library docking screening using plant-derived molecules, examining affinity energy, bond types, and interacting residues.

Molecular docking was conducted using MOE 2022.02 and a previously established method [19], employing the General docking scenario via MOE>Compute>Dock. Settings included Receptor and Solvent for the receptor, Ligand Atoms for both ligand and site, and the Amber10:EHT all-atom forcefield. The active site was defined by the SKM co-crystalline ligand's interaction with *Mt*SK, with binding pockets identified via command, Surface>Receptor. Docking followed a two-step protocol: initial ligand Placement using Triangle Matcher with London ΔG scoring, generating 30 poses, followed by refinement using rigid or induced fit receptors with GBVI/WSA ΔG scoring. The top five poses per ligand were retained. Docking was applied in both validation and compound screening stages.

2.6. Analysis and visualization of docking results.

The docking results were evaluated in terms of affinity energy and RMSD. The important parameter to examine during the re-docking phase is RMSD. A re-docking method is considered successful if the docked ligand has an RMSD of less than 2 Å. The affinity energy is the most important parameter to consider when performing control-compound docking and plant-compound library screening. Validation of control compounds is considered successful if the molecular docking system can group control compounds based on true conditions. Positive control compounds must have higher affinity energy than SKM ligands (more

negative), whereas negative controls must have lower affinity energy (more positive). A test compound is stated to have the ability to inhibit the *Mt*SK if it has a higher affinity energy than the SKM ligand. MOE 2022.02 will automatically display the affinity energy and RMSD parameters in the docking results output database. Docking results are visualized to facilitate the study of ligand-receptor interactions.

2.7. Pharmacophore screening.

Pharmacophore screening, performed in MOE 2022.02, filters compounds based on similarity to SKM ligand pharmacophore features. It involves two stages: creating a pharmacophore query using H-bond donor, acceptor, and donor projection features, and searching the compound library for matches. The query is built via MOE>Compute>Pharmacophore>Query Editor with EHT Scheme, and R-Strength enabled. Hits are identified using the Pharmacophore Search tool, and rscore is used to evaluate screening results. The Pharmacophore Search tool will run by pressing Search in the Pharmacophore Query Editor.

2.8. ADMET prediction.

ADME and drug-likeness predictions are used to determine a drug candidate's ability to be absorbed by the body, as well as its suitability as a drug candidate. The SwissADME website (http://www.swissadme.ch/) can estimate ADME and drug-likeness by entering SMILES and running the ADME prediction on the website. ADME predictions include gastrointestinal (GI) adsorption and blood-brain barrier (BBB) permeation, while drug-likeness is assessed using Lipinski's rule and Veber's rule. Toxicity prediction is used to evaluate the possible toxicity of a compound when consumed. Toxicity prediction is performed using the ProTox III website (https://tox.charite.de/protox3/) by entering SMILES and running the Start Tox-Prediction. The ProTox website states that Acute Toxicity (LD_{50}) is always computed.

3. Results and Discussion

3.1. Validation of molecular docking procedures.

Docking validation was performed in two distinct phases: re-docking of the native ligand (SKM) and docking of control compounds. In the re-docking phase, the native ligand exhibited mean RMSD values of 1.2378 ± 0.0005 Å and 1.5130 ± 0.4243 Å when docked using the rigid receptor and induced fit receptor protocols, respectively (Table 4). In the SKM–*Mt*SK complex, the hydroxyl moieties of SKM function as hydrogen bond donors to Asp34 and as hydrogen bond acceptors from Gly80. Additionally, the carboxyl group of SKM acts as a hydrogen-bond acceptor and forms ionic interactions with Arg58 and Arg136. These intermolecular contacts exhibit comparable bond distances to those observed in the native *Mt*SK conformation (Figures 2 and 3).

Redocking involved the extraction and subsequent reintroduction of the native ligand into the protein structure, with RMSD used to evaluate the accuracy of the ligand conformations (to quantify the alignment between the redocked and crystallographic ligand poses). In this study, RMSD values obtained with both rigid and induced-fit receptor docking methods were consistently below the threshold, thereby confirming the reliability and effectiveness of the docking strategy. Across repeated trials, the re-docked ligand consistently

reproduced key interaction patterns, maintaining similar bonding types and residue contacts. Notably, stable hydrogen bonding and ionic interactions were observed with Asp34, Arg58, Gly80, and Arg136, underscoring the reliability of the docking approach. Together, these four amino acid residues define the catalytic core of *Mt*SK, forming the essential structural framework required for enzymatic activity [20].

Table 4. Results of native ligand (SKM) re-docking.

Method	Binding energy (Δ*G*, kcal/mol)	RMSD (Å)	Bond type and interaction of amino acid residues with native ligands
Rigid receptor	-6.4269 ± 0.0032	1.2378 ± 0.0005	hydrogen bond donor: Asp34 hydrogen bond acceptor: Arg58, Gly80, Arg136 ionic bonds: Arg58, Arg136
Induced fit receptor	-6.3966 ± 0.0009	1.5130 ± 0.4243	

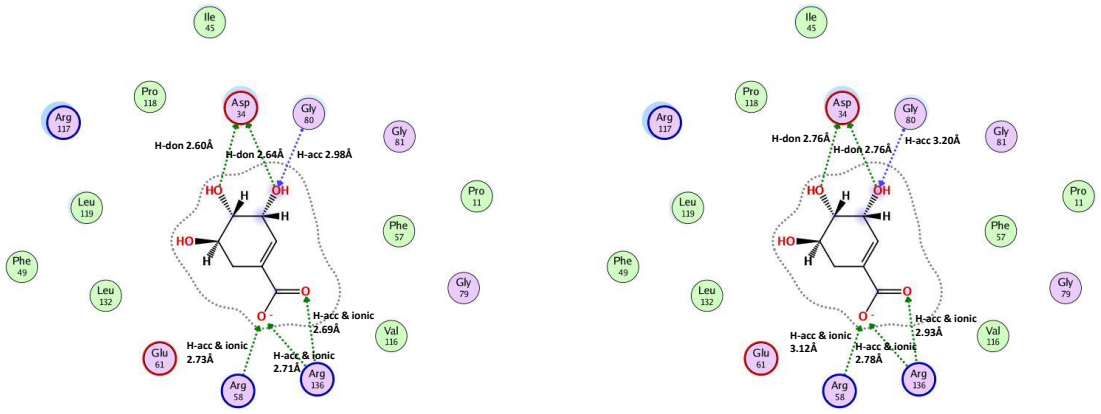

(a) **(b)**

Figure 2. Interaction of native ligand (SKM) with amino acid residues in re-docking with the rigid receptor method (**a**) before re-docking; (**b**) after re-docking. H-don: hydrogen bond donor, H-acc: hydrogen bond acceptor, ionic: ionic bond.

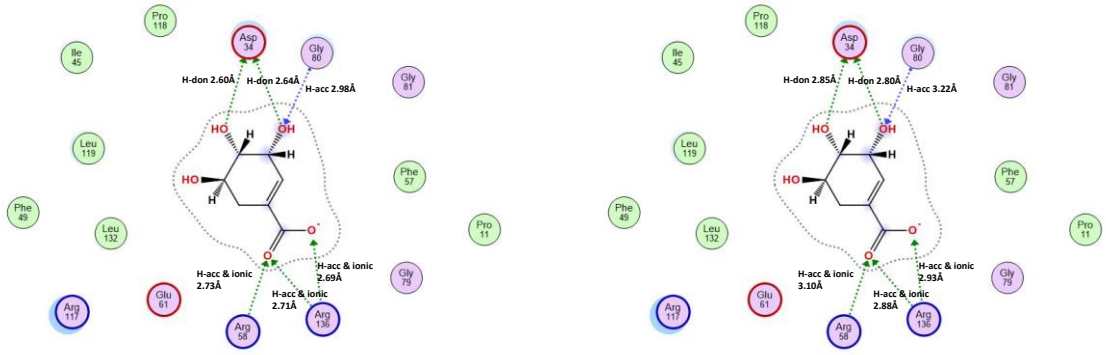

(a) **(b)**

Figure 3. Interaction of native ligand (SKM) with amino acid residues in re-docking with the induced fit receptor method **(a)** before re-docking; **(b)** after re-docking. H-don: hydrogen bond donor, H-acc: hydrogen bond acceptor, ionic: ionic bond.

To assess the predictive performance of the docking methodology, a validation set comprising 15 known *Mt*SK inhibitors (positive controls) and 163 decoy compounds (negative controls) was docked against the *Mt*SK receptor. Among the positive controls, 12 compounds exhibited binding affinities more favorable than that of SKM (<-6.4 kcal/mol), resulting in three false negatives. Conversely, 160 of the negative controls displayed binding energies less favorable than −6.4 kcal/mol, yielding three false positives. These results support the

discriminative capability of the docking protocol in distinguishing active inhibitors from inactive compounds.

The docking system correctly classified the majority of compounds, with only three false negatives and three false positives. The rigid receptor and induced fit receptor approaches achieved specificity values of 98.15% and 98.8%, respectively, and sensitivity values of 80% and 81.25%, respectively. These metrics confirm the robustness of the docking protocol in accurately identifying true inhibitors while minimizing erroneous predictions.

3.2. Virtual screening of MtSK inhibitors by molecular docking and pharmacophore screening.

Virtual screening of *Mt*SK inhibitors was conducted using compound libraries derived from the Asteraceae and Fabaceae families, employing both rigid and induced fit receptor docking approaches. Using the rigid receptor method, 1587 compounds from the Asteraceae library (Figure 4) and 2146 from the Fabaceae library (Figure 5) exhibited binding affinities lower than that of shikimate (–6.40 kcal/mol). The identified hits from Asteraceae displayed affinity energies ranging from –6.40 to –10.83 kcal/mol, while those from Fabaceae ranged from –6.40 to –12.47 kcal/mol. Similarly, the induced fit receptor method identified 1560 and 2098 compounds from the Asteraceae and Fabaceae libraries, respectively, with binding energies below the shikimate threshold. The corresponding affinity ranges were –6.44 to –12.78 kcal/mol for Asteraceae and –6.44 to –14.17 kcal/mol for Fabaceae, indicating a broader spectrum of potential inhibitors under induced fit receptor docking.

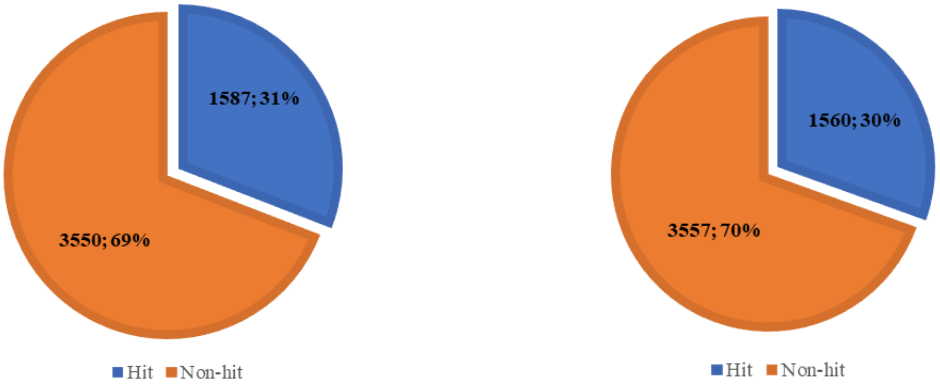

(a) **(b)**

Figure 4. Molecular docking results of the Asteraceae family chemical compound library: **(a)** rigid receptor docking; **(b)** induced fit receptor docking.

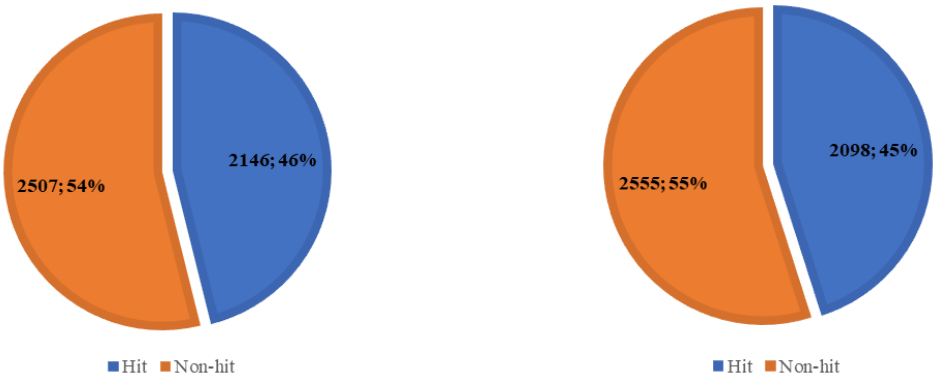

(a) **(b)**

Figure 5. Molecular docking results of the Fabaceae family chemical compound library: **(a)** rigid receptor docking; **(b)** induced fit receptor docking.

Molecular docking techniques facilitate the high-throughput screening of extensive chemical libraries by evaluating ligand-receptor interactions based on binding affinity. This virtual screening approach enables rapid, cost-effective assessment of thousands of compounds, serving as a preliminary filter before more resource-intensive experimental validation.

Despite promising initial results, further investigation is necessary to confirm the biological activity of the identified hit compounds. Molecular docking methodologies possess inherent limitations, including inaccuracies in scoring functions for binding affinity estimation and frequent errors in predicting ligand conformations within the receptor binding site. Consequently, compounds identified through virtual screening often fail to exhibit significant activity in subsequent in vitro and in vivo assays. To enhance confidence in the predicted activity and reduce the incidence of false positives, complementary screening techniques such as pharmacophore modeling are essential. Compounds exhibiting lower binding energies than control molecules are considered suitable candidates for subsequent pharmacophore-based evaluation.

Pharmacophore screening is a post-docking analytical approach that identifies candidate compounds exhibiting pharmacophoric congruence with reference ligands. In the present study, six pharmacophore features derived from SKM were used as screening templates (see Table 5). These features encompass hydrogen bond donors (F1 and F2) interacting with Asp34 and Gly80, hydrogen bond acceptors (F3 and F4) engaging Arg58 and Arg136, and hydrogen bond donor projections (F5 and F6) targeting Asp34. Collectively, these four amino acid residues constitute the catalytic site of *Mt*SK [20].

Table 5. SKM pharmacophore queries.

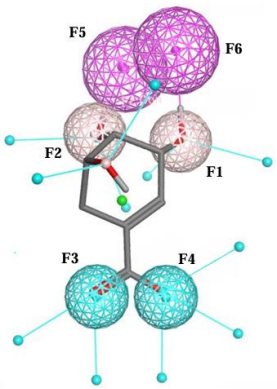

Pharmacophore code	Pharmacophore features	Amino acid residues involved
F1	H-bond donor	Asp34, Gly80
F2	H-bond donor	Asp 34
F3	H-bond acceptor	Arg58, Arg136
F4	H-bond acceptor	Arg136
F5	H-bond donor projection	Asp34
F6	H-bond donor projection	Asp34

Table 6. Pharmacophore screening results from the Asteraceae and Fabaceae database.

Compound	PubChem ID	Plant sources	rscore [1]	rscore favored [1]	Binding energy (Δ*G*, kcal/mol) [2]	
					Rigid	Induced Fit
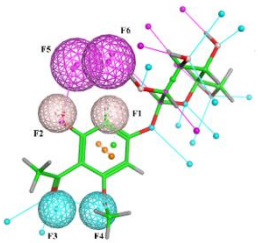 Annphenone (As1) [3]	15929152	*Artemisia annua*, *Artemisia capillaris*	22.0930	F2 (6.3319) F5 (6.3319) F6 (4.6927)	-7.6579	-8.2622

Compound	PubChem ID	Plant sources	rscore [1]	rscore favored [1]	Binding energy (ΔG, kcal/mol) [2]	
					Rigid	Induced Fit
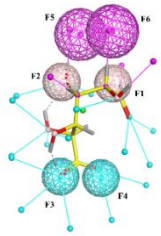 D-Galacturonic acid (As2) [3]	84740	*Helianthus annuus*	21.8837	F1 (3.2727) F3 (3.6642) F4 (3.6642)	-6.5353	-6.4489
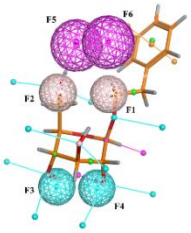 Phenylethyl β-D-glucopyranoside (As3) [3]	11289099	*Pluchea indica*	13.2761	-	-6.4775	-7.4140
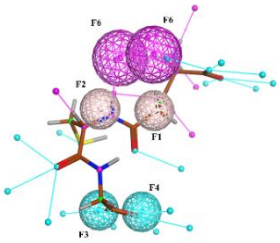 Glutathione (Fa1) [3]	124886	*Phaseolus vulgaris*	26.4751	F2 (7.2227) F5 (7.2227)	-7.9412	-8.2623
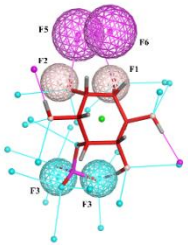 1D-myo-inositol 6-phosphate (Fa2) [3]	161368	*Phaseolus lunnatus*	25.5350	F1 (4.3195) F3 (4.0578) F4 (4.1994) F6 (4.3195)	-6.9829	-7.3820
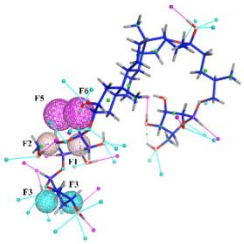 (Fa3) [3]	154497616	*Trigonella foenum-graecum*	10.2816	-	-8.1159	-10.5374

[1]pharmacophore screening; [2] docking screening; [3]letter: a compound from the Asteraceae (As) and Fabaceae (Fa) families; number: a compound number.

Pharmacophore-based virtual screening identified six candidate compounds, comprising three from the Asteraceae family database and three from the Fabaceae family database (Table 6). The Asteraceae-derived hits included annphenone (As1), galacturonic acid (As2), and phenylethyl β-D-glucopyranoside (As3), while the Fabaceae-derived hits consisted of glutathione (Fa1), 1D-myo-inositol 6-phosphate (Fa2), and an additional compound designated as Fa3.

Six hit compounds exhibiting pharmacophoric congruence with the previously characterized SKM were identified through pharmacophore screening. Among these, compounds As1 and As2 (Asteraceae) and Fa1 and Fa2 (Fabaceae) were prioritized based on their high rscore values and the number of favored features contributing to those scores. Compound As1 (rscore = 22.0930) showed major contributions from hydrogen bond donor features F2, F5, and F6, while compound As2 (rscore = 21.8837) was primarily influenced by hydrogen bond donor feature F1, and hydrogen bond acceptor features F3 and F4. In the Fabaceae dataset, compound Fa1 (rscore = 26.4751) was driven by hydrogen bond donor features F2 and F5, and compound Fa2 (rscore = 25.5350) by hydrogen bond donor features F1 and F6, and hydrogen bond acceptor features F3 and F4. The rscore reflects the cumulative similarity across all pharmacophoric features relative to SKM, whereas the favored rscore denotes the highest individual feature contribution [21].

Compounds Fa3, Fa1, and As1 demonstrated the most favorable binding interactions with the target protein, as indicated by their highly negative binding energies in both rigid and induced fit docking simulations. In rigid receptor docking, the binding energies were −8.1159, −7.9412, and −7.6579 kcal/mol, respectively, while induced fit docking yielded values of −10.5374, −8.2623, and −8.2622 kcal/mol. These results suggest strong ligand–receptor complementarity and imply that these compounds are the most potent inhibitors among the screened candidates. Conversely, compounds As2, As3, and Fa2 exhibited less negative binding energies, reflecting comparatively weaker affinities.

3.3. ADMET prediction.

The ADMET analysis underscores the potential of As3 as a promising lead, given its superior predicted absorption capacity (Table 7). Compliance of As1, As2, As3, Fa1, and Fa2 with Lipinski's criteria, alongside the additional fulfillment of Veber's rules by As2 and As3, highlights their favorable physicochemical properties for oral administration. Importantly, the non-toxic classification of five out of six lead compounds (As1, As2, As3, Fa1, and Fa2) suggests a reassuring safety margin, thereby strengthening their candidacy for further preclinical evaluation (Table 8). Collectively, these results indicate that As2 and As3, in particular, combine optimal pharmacokinetic predictions with drug-likeness and safety attributes, positioning them as strong candidates for prioritization in subsequent optimization and experimental validation.

Evaluation of compound compliance with Lipinski's and Veber's rules provides predictive insight into their drug-likeness. Lipinski's rule of five assesses bioavailability based on molecular weight, partition coefficient, and the number of hydrogen bond donors and acceptors, with compounds considered acceptable if they meet at least three of the four criteria [22]. Compounds As1, As2, As3, and Fa1 fully comply with Lipinski's parameters, while Fa2 violates a single criterion but remains within the permissible threshold of one infringement. In contrast, Fa3 fails to meet Lipinski's requirements, breaching three of the four conditions, with a molecular weight of 907 g/mol, 19 hydrogen bond acceptors, and 12 hydrogen bond donors. Lipinski's framework further emphasizes that molecules with molecular weights below 500 are typically suitable as medicinal agents; accordingly, As1, As2, As3, and Fa1 meet this benchmark. Their substantial numbers of hydrogen bond donors and acceptors also suggest favorable solubility and strong potential for biological interactions.

Veber's rule provides an additional measure of oral bioavailability, focusing on topological polar surface area (TPSA) and molecular flexibility, as indicated by rotatable

bonds. A compound is considered compliant only if both criteria are satisfied. Among the tested compounds, only As2 and As3 fully adhere to Veber's requirements. By contrast, As1, Fa1, and Fa2 exhibit TPSA values exceeding 140 Å², while Fa3 fails to meet all Veber parameters. Elevated TPSA values (>140 Å²) are associated with poor absorption and limited ability to traverse cell membranes during oral administration. Furthermore, the number of rotatable bonds directly influences molecular flexibility, which in turn affects binding efficiency.

Table 7. ADME prediction results for hit compounds.

Compound	Lipinski's rule				Veber's rule	
	MW (<500)	Partition coefficient (WlogP<5)	H-bond acceptors (≤10)	H-bond donors (≤5)	TPSA (<140 Å²)	Rotatable bond (≤10)
As1	344.31	-1.22	9	5	145.91	5
As2	194.14	-3.29	7	5	135.29	5
As3	284.31	-0.95	6	4	99.38	5
Fa1	307.32	-2.21	7	2	197.62	9
Fa2	260.14	-3.72	9	7	177.72	2
Fa3	907.0	-2.17	19	12	307.37	12

Table 8. Prediction of the toxicity of hit compounds.

Compound	LD_{50} (mg/kg)	Acute toxicity category
As1	3750	5 (may be harmful if swallowed)
As2	9100	not toxic
As3	6000	not toxic
Fa1	5000	5 (may be harmful if swallowed)
Fa2	9300	not toxic
Fa3	50	2 (fatal if swallowed)

ADME prediction was employed to evaluate the absorption potential of candidate compounds based on pharmacokinetic properties [23]. In this study, gastrointestinal (GI) absorption and blood–brain barrier (BBB) permeability were assessed using the Brain Or IntestinaL EstimateD (BOILED-Egg) model implemented in SwissADME. This model estimates compound distribution within the body according to polarity and lipophilicity [24,25]. Structurally, the model resembles an egg, with the white region denoting the likelihood of GI absorption and the yolk representing the probability of BBB penetration following oral administration [26]. Application of the BOILED-Egg model to the Asteraceae dataset identified only compound As3 (Figure 6). As3 was positioned within the egg white, suggesting efficient absorption through the digestive tract. Compounds with high GI absorption are generally more readily absorbed in the intestine, thereby enhancing oral bioavailability. Consistent with this, As3 demonstrated strong absorption capacity, supporting its potential as a promising oral therapeutic candidate.

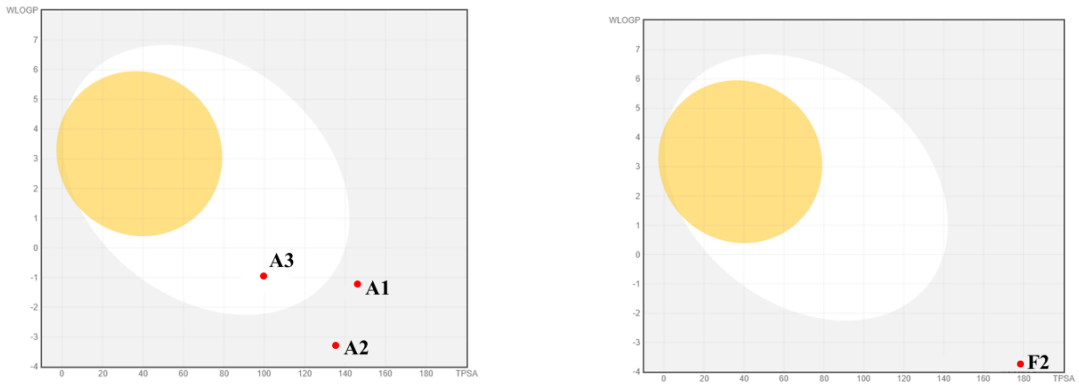

(a) **(b)**

Figure 6. A BOILED-Egg graph of hit compounds from the **(a)** Asteraceae; **(b)** Fabaceae families.

In contrast, the remaining compounds displayed limited absorption, which may constrain their suitability for oral administration. Furthermore, none of the tested compounds were predicted to cross the BBB, indicating restricted applicability for central nervous system–targeted therapies.

SwissADME provides a graphical representation of six key physicochemical parameters influencing oral bioavailability through the bioavailability radar—a hexagonal plot encompassing lipophilicity, molecular size, polarity, solubility, saturation, and molecular flexibility. The magenta-shaded region delineates the optimal range for each parameter based on reference standards. Among the evaluated compounds, compound As3 uniquely satisfies all six physicochemical parameters within the optimal range defined by the SwissADME bioavailability radar, thereby reinforcing its potential for efficient oral absorption and favorable pharmacokinetic behavior, as illustrated in Figure 7.

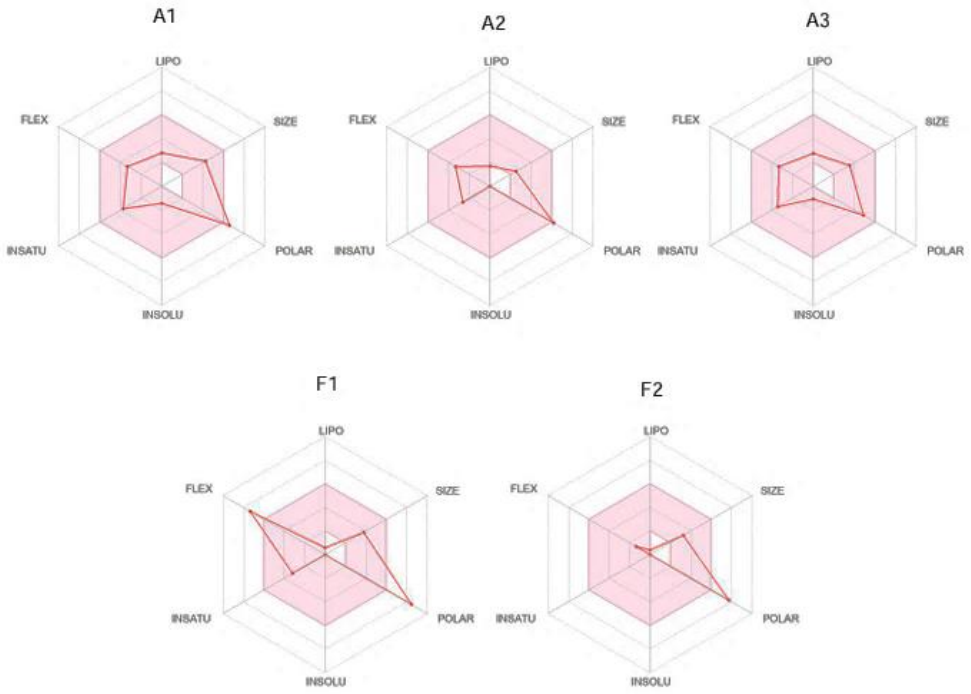

Figure 7. Oral bioavailability radar for hit compounds.

Toxicity evaluation revealed that compounds As1, As2, As3, Fa1, and Fa2 were classified as non-toxic, with LD_{50} values ranging from category 5 (2000–5000 mg/kg) to >5000 mg/kg, indicating relatively low acute toxicity or complete safety. In contrast, compound Fa3 was assigned to Category 2 (5–50 mg/kg), signifying high acute toxicity and fatal risk upon ingestion.

According to ADMET prediction outcomes, compound Fa3 was excluded from subsequent evaluation as a potential *Mt*SK inhibitor.

3.4. Hit compounds from virtual screening using molecular docking, pharmacophore evaluation, and ADMET prediction.

Molecular docking analysis demonstrated that annphenone (As1) exhibits binding affinities of −7.6579 kcal/mol and −8.2622 kcal/mol with *Mt*SK under rigid and induced-fit receptor models, respectively. Structurally, annphenone contains a single carbonyl group and five hydroxyl moieties (Figure 8). Within the annphenone–*Mt*SK complex, one hydroxyl group

donates a hydrogen bond to Asp34, while the ring oxygen, an additional hydroxyl group, and two carbonyl groups act as hydrogen bond acceptors, forming interactions with Arg117, Lys15, Arg58, and Arg136. The stabilization of the complex is primarily mediated by hydrogen bonding between the hydroxyl group and Asp34, as well as the carbonyl group and Arg58, which constitute the dominant interactions. The hydroxyl moiety of annphenone, which engages Asp34, shows pharmacophoric similarity to SKM, which interacts with the same residue. Furthermore, annphenone establishes contacts with three of the four critical amino acids of *Mt*SK—Asp34, Arg58, and Arg136—each essential for ligand recognition and binding. These interactions collectively highlight annphenone's potential as a promising *Mt*SK inhibitor. Although annphenone complies with all parameters of Lipinski's rule, it fails to meet Veber's criteria due to its TPSA exceeding the recommended threshold and may limit its oral absorption efficiency [27]. Annphenone is a phenolic compound naturally occurring in several species of the Artemisia genus (Asteraceae), notably *Artemisia annua* and *Artemisia capillaris*. It is predominantly localized in the aerial parts of these plants, including the stems, leaves, and flowers [28,29]. Ethnobotanical reports from communities in Brazil and Africa indicate the use of *Artemisia* species in traditional remedies for tuberculosis [7,10].

Molecular docking analysis revealed that galacturonic acid (As2) binds to *Mt*SK with affinity energies of −6.5353 kcal/mol and −6.4489 kcal/mol under rigid and induced-fit receptor models, respectively. Structurally, galacturonic acid contains an aldehyde group, a carboxyl group, and four hydroxyl moieties (Figure 8). Within the galacturonic acid–*Mt*SK complex, one hydroxyl group donates a hydrogen bond to Asp34, while a carbonyl group and another hydroxyl group act as hydrogen bond acceptors, forming interactions with Arg58 and Gly80. The carboxyl group serves as a hydrogen bond acceptor and simultaneously establishes ionic interactions with Arg58 and Arg136. Stabilization of the complex is therefore primarily mediated by hydrogen bonding with Asp34 and carboxyl-driven interactions involving Arg58 and Arg136. The hydroxyl group engaging Asp34 reflects pharmacophoric similarity to SKM, which interacts with the same residue, while the carboxyl group mirrors SKM's pharmacophoric role in binding Arg58 and Arg136. Collectively, galacturonic acid interacts with all four critical amino acids of *Mt*SK—Asp34, Arg58, Gly80, and Arg136—known to be essential for SKM–*Mt*SK ligand recognition and binding. In terms of drug-likeness, galacturonic acid complies fully with both Lipinski's and Veber's rules. Toxicity evaluation indicated it as non-toxic. Nonetheless, its bioavailability remains unverified, necessitating further investigation to confirm absorption efficiency upon oral administration. Galacturonic acid is a carbohydrate molecule that is the primary constituent of pectin in plants, including sunflowers (*Helianthus annuus*). The Mayo community in Mexico used this plant to treat tuberculosis [10,30]. Sunflower stem extract demonstrated antimycobacterial action against *M. tuberculosis* H37Rv, with a MIC value of 250-500 µg/ml. The synthetic chemical d-galacturonic acid isonicotinyl hydrazide, which combines galacturonic acid and isonicotinyl hydrazide, has antituberculosis activity against *M. tuberculosis* H37Rv [31].

Molecular docking analysis demonstrated that phenylethyl β-D-glucopyranoside (As3) binds to *Mt*SK with affinity energies of −6.4775 kcal/mol and −7.4140 kcal/mol under rigid and induced-fit receptor models, respectively. Structurally, the compound contains four hydroxyl groups (Figure 8). Within the phenylethyl β-D-glucopyranoside–*Mt*SK complex, one hydroxyl group donates a hydrogen bond to Asp34, while the remaining hydroxyl groups act as hydrogen bond acceptors, forming interactions with Gly80, Arg58, Leu119, and Arg136. Stabilization of the complex is primarily mediated through hydrogen bonding with Asp34,

Gly80, and Arg136. The hydroxyl group engaging Asp34 reflects pharmacophoric similarity to SKM, which interacts with the same residue, whereas additional hydroxyl groups mirror the pharmacophoric role of SKM's carboxyl group by engaging Arg58 and Arg136. Collectively, phenylethyl β-D-glucopyranoside interacts with three of the four critical amino acids of *Mt*SK—Asp34, Gly80, and Arg136—known to be essential for SKM–*Mt*SK ligand recognition, thereby supporting its potential as a promising inhibitory candidate. In terms of drug-likeness, the compound complies fully with Lipinski's and Veber's rules, as well as the physicochemical parameters of the BOILED-Egg model and bioavailability radar. Toxicity evaluation indicated it as non-toxic. These findings suggest that phenylethyl β-D-glucopyranoside may serve as a safe and orally bioavailable *Mt*SK inhibitor. *Pluchea indica* (Asteraceae), commonly known as beluntas, contains the phenolic compound phenylethyl β-D-glucopyranoside, which is distributed throughout the plant's aerial parts, including stems, leaves, and flowers [32]. Traditionally, this species has been employed by local communities in Indonesia for the treatment of tuberculosis [33].

Molecular docking analysis revealed that glutathione (Fa1) binds to *Mt*SK with affinity energies of −7.9412 kcal/mol under the rigid receptor model and −8.2623 kcal/mol using the induced-fit approach. Structurally, glutathione comprises two carboxyl groups, two carbonyl groups, two –NH– groups, one –SH group, and an NH_3^+ moiety (Figure 8). Within the glutathione–*Mt*SK complex, the NH_3^+ group donates a hydrogen bond to Ser16 while simultaneously forming ionic interactions with Asp32 and Asp34. One carboxyl group engages Lys15 through ionic contacts, whereas another carboxyl group and the –SH moiety act as hydrogen bond acceptors, interacting with Ser16 and Arg58, respectively. The carboxyl groups additionally contribute as hydrogen bond acceptors and establish ionic interactions with Arg58, Arg117, and Arg136. The NH_3^+ group's interaction with Asp34 reflects pharmacophoric similarity to the hydroxyl moiety of SKM, which binds the same residue, while the –SH group parallels the pharmacophoric role of SKM's carboxyl group through its interaction with Arg58. Collectively, glutathione engages three of *Mt*SK's critical residues—Asp34, Arg58, and Arg136—known to be central to SKM–*Mt*SK ligand recognition, thereby underscoring its potential as a strong inhibitory candidate. In terms of drug-likeness, glutathione complies with Lipinski's rule of five. Still, it fails to meet Veber's criteria due to its elevated TPSA and high bond flexibility, which may hinder oral absorption. This limitation is consistent with findings by Giustarini et al., who reported that oral glutathione has poor bioavailability because it is typically degraded in the intestinal tract before absorption [34]. Consequently, alternative routes of administration must be considered to ensure its therapeutic efficacy. Glutathione, an alkaloid compound widely distributed in various plants and fruit species, has been identified in the roots of *Phaseolus vulgaris*, a member of the Fabaceae family. Ethnobotanical accounts from Uganda suggest that *P. vulgaris* has been traditionally utilized in the treatment of tuberculosis [8].

Molecular docking analysis indicated that 1D-myo-inositol 6-phosphate (Fa2) binds to *Mt*SK with affinity energies of −6.9829 kcal/mol and −7.3820 kcal/mol under rigid and induced-fit receptor models, respectively. Structurally, the compound comprises five hydroxyl groups and a phosphate ion (Figure 8). Within the 1D-myo-inositol 6-phosphate–*Mt*SK complex, two hydroxyl groups donate hydrogen bonds to Asp34, while additional hydroxyl groups act as hydrogen bond acceptors, forming interactions with Arg58, Gly80, and Gly81. The phosphate ion also functions as a hydrogen bond acceptor, interacting with Pro11, and contributes to stabilization through simultaneous ionic contacts with Arg58 and Arg136. The

hydroxyl groups engaging Asp34 reflect pharmacophoric similarity to SKM, which interacts with the same residue, while the phosphate ion parallels the pharmacophoric role of SKM's carboxyl group by binding Arg58 and Arg136. Collectively, 1D-myo-inositol 6-phosphate interacts with all four critical amino acids of *Mt*SK—Asp34, Arg58, Gly80, and Arg136—known to mediate SKM–*Mt*SK ligand recognition, thereby underscoring its potential as a strong inhibitory candidate. In terms of drug-likeness, the compound violates one Lipinski criterion, with seven hydrogen bond acceptors exceeding the recommended limit of five. It also fails to meet Veber's rule due to its elevated TPSA, which surpasses the threshold, suggesting limited oral absorption [27].

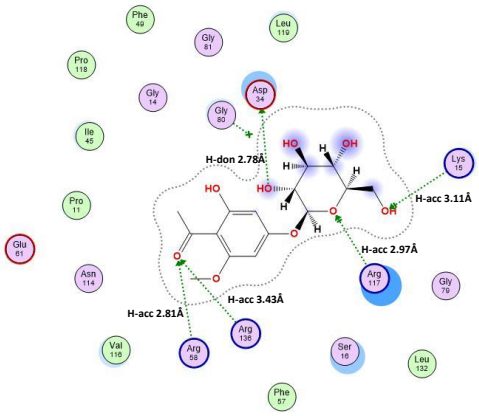

Annphenone - rigid receptor

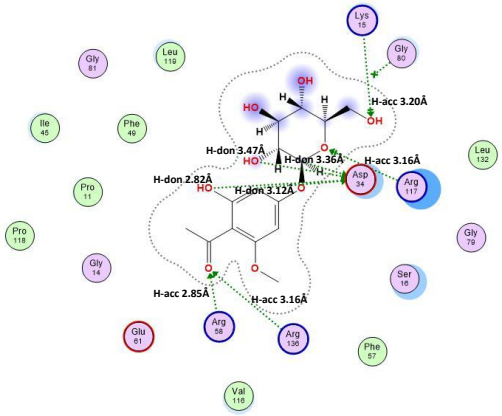

Annphenone – induced fit receptor

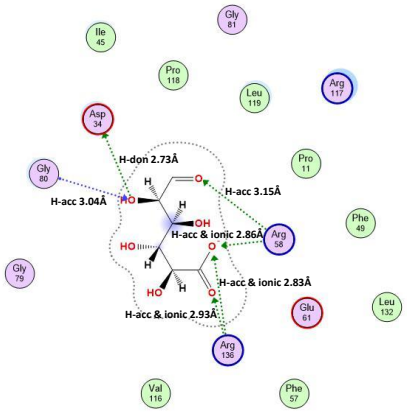

Galacturonic acid - rigid receptor

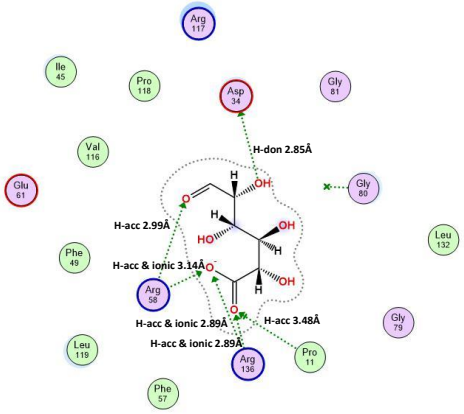

Galacturonic acid – induced fit receptor

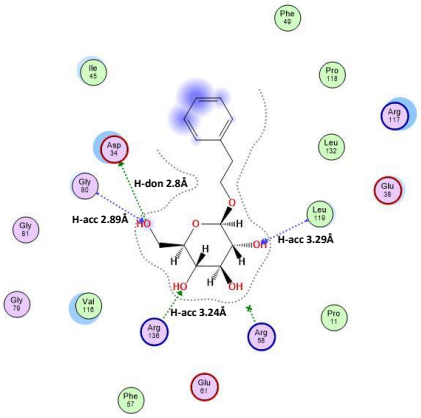

Phenylethyl β-D-glucopyranoside - rigid receptor

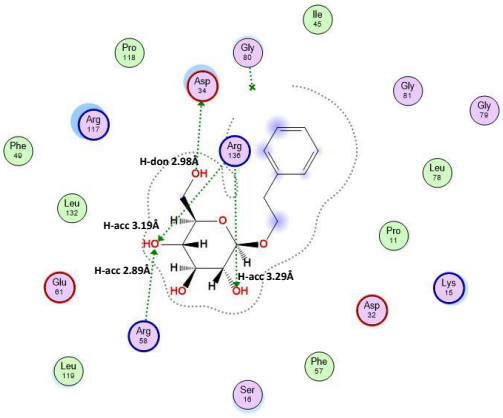

Phenylethyl β-D-glucopyranoside – induced fit receptor

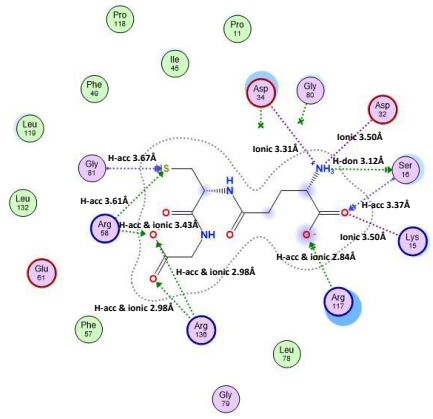

Glutathione - rigid receptor

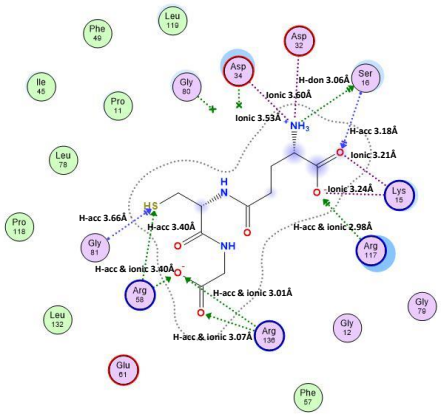

Glutathione – induced fit receptor

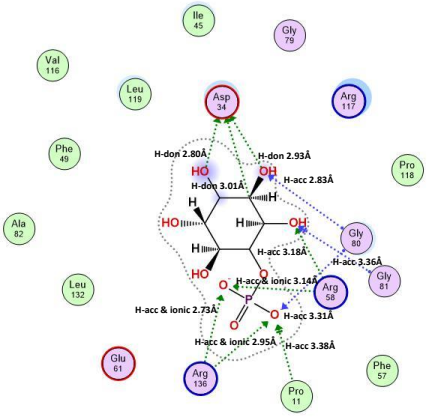

1D-myo-inositol 6-phosphate - rigid receptor

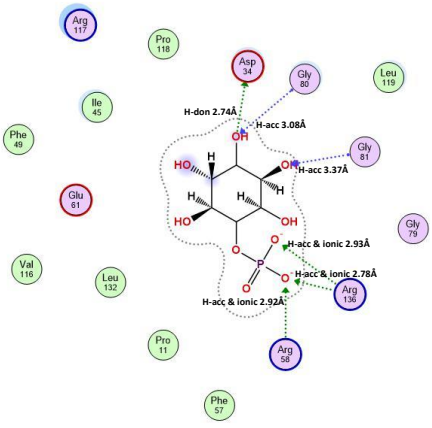

1D-myo-inositol 6-phosphate - induced fit receptor

Figure 8. Binding of hit compounds with the *Mt*SK receptor. H-don: hydrogen bond donor, H-acc: hydrogen bond acceptor, ionic: ionic bond.

Toxicity assessment classifies the compound as non-toxic. 1D-myo-inositol 6-phosphate is an inositol phosphate group molecule present in a variety of foods, including fruits and nuts. This chemical is found in various plants of the Fabaceae family, including *Sphenostylis stenocarpa*, *Canavalia ensiformis*, *Phaseolus lunatus*, and *Cajanus cajan* [35]. Ethnobotanical records indicate that *P. lunatus* has been traditionally used in Uganda to treat tuberculosis [8].

Molecular docking analyses revealed distinct binding profiles among the tested compounds, with glutathione (Fa1) and annphenone (As1) exhibiting the strongest affinities toward *Mt*SK (−7.94/−8.26 kcal/mol and −7.65/−8.26 kcal/mol, respectively), while galacturonic acid (As2), phenylethyl β-D-glucopyranoside (As3), and 1D-myo-inositol 6-phosphate (Fa2) demonstrated moderate binding energies ranging between −6.44 and −7.41 kcal/mol. Despite these differences in affinity, all compounds established pharmacophoric congruence with SKM, particularly through hydrogen bonding with Asp34 and complementary interactions with Arg58 and Arg136, residues critical for ligand recognition.

Annphenone's stabilization was dominated by hydroxyl and carbonyl-mediated interactions with Asp34 and Arg58, engaging three of the four key residues, whereas galacturonic acid achieved broader residue coverage, binding all four critical amino acids (Asp34, Arg58, Gly80, Arg136) through hydroxyl and carboxyl-driven contacts. Phenylethyl β-D-glucopyranoside similarly interacted with Asp34, Gly80, and Arg136, reflecting SKM's pharmacophoric features, while glutathione engaged Asp34, Arg58, and Arg136 through NH_3^+ and –SH mediated interactions, underscoring its strong inhibitory potential. In contrast, 1D-

myo-inositol 6-phosphate displayed extensive residue engagement, including Asp34, Arg58, Gly80, and Arg136, with phosphate-mediated ionic contacts enhancing stabilization. These differences highlight how subtle variations in functional group composition—carbonyl, carboxyl, or hydroxyl—can markedly influence the strength and specificity of ligand–protein interactions. These findings provide valuable mechanistic insights for rational inhibitor design, suggesting that incorporating functional groups capable of engaging both hydrogen bonding and ionic interactions may yield compounds with superior binding affinity and selectivity toward *Mt*SK.

Drug-likeness evaluations further differentiated the candidates. Annphenone satisfied Lipinski's rule but failed Veber's due to its elevated TPSA (145.91 Å²), suggesting limited oral absorption. Galacturonic acid and phenylethyl β-D-glucopyranoside complied fully with both Lipinski's and Veber's rules, with the latter also aligning with BOILED-Egg and bioavailability radar predictions, supporting its potential as a safe and orally bioavailable inhibitor. Glutathione, despite strong binding, violated Veber's criteria (TPSA: 197.62 Å²; 11 rotatable bonds), consistent with reports of poor oral bioavailability due to intestinal degradation. Similarly, 1D-myo-inositol 6-phosphate breached one Lipinski parameter and Veber's TPSA threshold (177.72 Å²), indicating absorption challenges despite its non-toxic profile. Toxicity assessments classified all compounds as non-toxic, with LD_{50} values ranging from 6,000 mg/kg (phenylethyl β-D-glucopyranoside) to 9,300 mg/kg (1D-myo-inositol 6-phosphate).

4. Conclusions

Glutathione and annphenone exhibit superior binding affinities but face pharmacokinetic limitations, whereas galacturonic acid and phenylethyl β-D-glucopyranoside balance moderate binding with favorable drug-likeness and safety profiles. 1D-myo-inositol 6-phosphate demonstrates broad residue engagement yet is hindered by absorption constraints. These findings highlight phenylethyl β-D-glucopyranoside and galacturonic acid as promising orally bioavailable *Mt*SK inhibitor candidates, while glutathione and annphenone may require structural optimization or alternative delivery routes to overcome pharmacokinetic barriers. These inhibitors show promise as candidates for the development of a new anti-tuberculosis therapy and warrant additional in vitro and in vivo experiments to establish their biological efficacy, selectivity, safety, bioavailability, and metabolic stability. As this study was limited to in silico analyses, subsequent in vitro and in vivo validation is indispensable to confirm the inhibitors' therapeutic potential.

Author Contributions

Conceptualization, N.B.N. and A.A.; methodology, N.B.N. and F.N.; software, N.B.N. and F.N.; validation, N.B.N. and F.N.; formal analysis, F.N.; investigation, F.N.; resources, N.B.N. and F.N.; data curation, N.B.N. and F.N.; writing—original draft preparation, N.B.N.; writing—review and editing, N.B.N. and A.A.; visualization, F.N.; supervision, N.B.N. and A.A. All authors have read and agreed to the published version of the manuscript.

Institutional Review Board Statement

Not applicable.

Informed Consent Statement

Not applicable.

Data Availability Statement

Data supporting the findings of this study are available upon reasonable request from the corresponding author.

Funding

This research received no external funding.

Acknowledgments

The contributors to this work, whether directly or indirectly, have our sincere gratitude.

Conflicts of Interest

The authors declare no conflict of interest.

References

1. World Health Organization. Global Tuberculosis Report 2024, 1st ed.; World Health Organization: Geneva, Switzerland, **2004**; pp. 2.
2. Nunes, J.E.S.; Duque, M.A.; de Freitas, T.F.; Galina, L.; Timmers, L.F.S.M.; Bizarro, C.V.; Machado, P.; Basso, L.A.; Ducati, R.G. *Mycobacterium tuberculosis* Shikimate Pathway Enzymes as Targets for the Rational Design of Anti-Tuberculosis Drugs. *Molecules* **2020**, *25*, 1259, https://doi.org/10.3390/molecules25061259.
3. Almeida, A.M.; Marchiosi, R.; Abrahão, J.; Constantin, R.P.; dos Santos, W.D.; Ferrarese-Filho, O. Revisiting the shikimate pathway and highlighting their enzyme inhibitors. *Phytochem. Rev.* **2024**, *23*, 421-457, https://doi.org/10.1007/s11101-023-09889-6.
4. Zhang, Yanjia J.; Reddy, Manchi C.; Ioerger, Thomas R.; Rothchild, Alissa C.; Dartois, V.; Schuster, Brian M.; Trauner, A.; Wallis, D.; Galaviz, S.; Huttenhower, C.; Sacchettini, James C.; Behar, Samuel M.; Rubin, Eric J. Tryptophan Biosynthesis Protects Mycobacteria from CD4 T-Cell-Mediated Killing. *Cell* **2013**, *155*, 1296-1308, https://doi.org/10.1016/j.cell.2013.10.045.
5. Rios-Soto, L.; Hernández-Campos, A.; Tovar-Escobar, D.; Castillo, R.; Sierra-Campos, E.; Valdez-Solana, M.; Téllez-Valencia, A.; Avitia-Domínguez, C. Inhibition of Shikimate Kinase from Methicillin-Resistant *Staphylococcus aureus* by Benzimidazole Derivatives. Kinetic, Computational, Toxicological, and Biological Activity Studies. *Int. J. Mol. Sci.* **2024**, *25*, 5077, https://doi.org/10.3390/ijms25105077.
6. Raqib, R.; Sarker, P. Repurposed Drugs and Plant-Derived Natural Products as Potential Host-Directed Therapeutic Candidates for Tuberculosis. *Biomolecules* **2024**, *14*, 1497, https://doi.org/10.3390/biom14121497.
7. Getachew, S.; Medhin, G.; Asres, A.; Abebe, G.; Ameni, G. Traditional medicinal plants used in the treatment of tuberculosis in Ethiopia: A systematic review. *Heliyon* **2022**, *8*, e09478, https://doi.org/10.1016/j.heliyon.2022.e09478.
8. Obakiro, S.B.; Kiprop, A.; Kowino, I.; Kigondu, E.; Odero, M.P.; Omara, T.; Bunalema, L. Ethnobotany, ethnopharmacology, and phytochemistry of traditional medicinal plants used in the management of symptoms of tuberculosis in East Africa: a systematic review. *Trop. Med. Health* **2020**, *48*, 68, https://doi.org/10.1186/s41182-020-00256-1.
9. Sharifi-Rad, J.; Salehi, B.; Stojanović-Radić, Z.Z.; Fokou, P.V.T.; Sharifi-Rad, M.; Mahady, G.B.; Sharifi-Rad, M.; Masjedi, M.-R.; Lawal, T.O.; Ayatollahi, S.A.; Masjedi, J.; Sharifi-Rad, R.; Setzer, W.N.; Sharifi-Rad, M.; Kobarfard, F.; Rahman, A.-u.; Choudhary, M.I.; Ata, A.; Iriti, M. Medicinal plants used in the treatment of tuberculosis - Ethnobotanical and ethnopharmacological approaches. *Biotechnol. Adv.* **2020**, *44*, 107629, https://doi.org/10.1016/j.biotechadv.2020.107629.

10. Xu, Y.; Liang, B.; Kong, C.; Sun, Z. Traditional Medicinal Plants as a Source of Antituberculosis Drugs: A System Review. *BioMed Res. Int.* **2021**, *2021*, 9910365, https://doi.org/10.1155/2021/9910365.
11. Gupta, V.K.; Kumar, M.M.; Bisht, D.; Kaushik, A. Plants in our combating strategies against *Mycobacterium tuberculosis*: progress made and obstacles met. *Pharm. Biol.* **2017**, *55*, 1536-1544, https://doi.org/10.1080/13880209.2017.1309440.
12. Fasooto, T.T.; Ogundana, O.R.; Adebayo, A.F.; Olawade, D.B.; Olugbogi, E.A.; Fapohunda, O.; Akinmoladun, A.C. *In-silico* and *in-vivo* comparative evaluation of the cardioprotective potential of Yellow turmeric and White turmeric in Mn-induced cardiac oxidative stress. *Pharmacol. Res. Mod. Chin. Med.* **2024**, *10*, 100399, https://doi.org/10.1016/j.prmcm.2024.100399.
13. Sanusi, S.B.; Abu Bakar, M.F.; Mohamed, M.; Sabran, S.F.; Mainasara, M.M. Southeast Asian Medicinal Plants as a Potential Source of Antituberculosis Agent. *Evid. -Based Complement. Altern. Med.* **2017**, *2017*, 7185649, https://doi.org/10.1155/2017/7185649.
14. Pernas, M.; Blanco, B.; Lence, E.; Thompson, P.; Hawkins, A.R.; González-Bello, C. Synthesis of rigidified shikimic acid derivatives by ring-closing metathesis to imprint inhibitor efficacy against shikimate kinase enzyme. *Org. Chem. Front.* **2019**, *6*, 2514-2528, https://doi.org/10.1039/C9QO00562E.
15. Masoko, P.; Mabusa, I.H.; Howard, R.L. Isolation of alpha-linolenic acid from Sutherlandia frutescens and its inhibition of *Mycobacterium tuberculosis'* shikimate kinase enzyme. *BMC Complement. Med. Ther.* **2016**, *16*, 366, https://doi.org/10.1186/s12906-016-1344-1.
16. Simithy, J.; Fuanta, N.R.; Hobrath, J.V.; Kochanowska-Karamyan, A.; Hamann, M.T.; Goodwin, D.C.; Calderón, A.I. Mechanism of irreversible inhibition of *Mycobacterium tuberculosis* shikimate kinase by ilimaquinone. *Biochim. Biophys. Acta Proteins Proteom.* **2018**, *1866*, 731-739, https://doi.org/10.1016/j.bbapap.2018.04.007.
17. Pandey, S.; Chatterjee, A.; Jaiswal, S.; Kumar, S.; Ramachandran, R.; Srivastava, K.K. Protein kinase C-δ inhibitor, Rottlerin inhibits growth and survival of mycobacteria exclusively through Shikimate kinase. *Biochem. Biophys. Res. Commun.* **2016**, *478*, 721-726, https://doi.org/10.1016/j.bbrc.2016.08.014.
18. Vianna, C.P.; de Azevedo, W.F. Identification of new potential *Mycobacterium tuberculosis* shikimate kinase inhibitors through molecular docking simulations. *J. Mol. Model.* **2012**, *18*, 755-764, https://doi.org/10.1007/s00894-011-1113-5.
19. Nugroho, N.B.; Etika, B.; Rahayu, S.T.; Wibowo, A.; Siska, E. Identifying lead compounds for potential anti-tuberculosis drugs by in silico *Mycobacterium tuberculosis* shikimate kinase inhibitors selection of chemical library. *Int. J. Appl. Pharm.* **2025**, *17*, 423-431, https://doi.org/10.22159/ijap.2025v17i2.52759.
20. Vikrant Singh, R.; Ashish, R.; Inshad Ali, K. Shikimate Kinase Inhibitors: An Update on Promising Strategy against *Mycobacterium tuberculosis*. *Curr. Drug Targets* **2023**, *24*, 388-405, https://doi.org/10.2174/1389450124666230208102645.
21. Elbaramawi, S.S.; Eissa, A.G.; Noureldin, N.A.; Simons, C. Exploring *Proteus mirabilis* Methionine tRNA Synthetase Active Site: Homology Model Construction, Molecular Dynamics, Pharmacophore and Docking Validation. *Pharmaceuticals* **2023**, *16*, 1263, https://doi.org/10.3390/ph16091263.
22. Samukelisiwe, N.; Musawenkosi Hope Lotriet, N.; Brendeline Linah, N.; Thabile, D.; Arnesh, T.; Inderasan, M.; Andre, V.; Uche, A.K.C.-O. Druggability of Pharmaceutical Compounds Using Lipinski Rules with Machine Learning. *Sci. Pharm*. **2024**, *3*, 177–192, https://doi.org/10.58920/sciphar0304264.
23. Yadav, R.; Imran, M.; Dhamija, P.; Chaurasia, D.K.; Handu, S. Virtual screening, ADMET prediction and dynamics simulation of potential compounds targeting the main protease of SARS-CoV-2. *J. Biomol. Struct. Dyn.* **2021**, *39*, 6617-6632, https://doi.org/10.1080/07391102.2020.1796812.
24. Daina, A.; Zoete, V. A BOILED-Egg To Predict Gastrointestinal Absorption and Brain Penetration of Small Molecules. *ChemMedChem* **2016**, *11*, 1117-1121, https://doi.org/10.1002/cmdc.201600182.
25. Sączewski, J.; Popenda, Ł.; Fedorowicz, J. In Silico SwissADME Analysis of Antibacterial NHC–Silver Acetates and Halides Complexes. *Appl. Sci.* **2024**, *14*, 8865, https://doi.org/10.3390/app14198865.
26. Al Azzam, K.M.; Negim, E.-S.; Aboul-Enein, H.Y. ADME studies of TUG-770 (a GPR-40 inhibitor agonist) for the treatment of type 2 diabetes using SwissADME predictor: In silico study. *J. Appl. Pharm. Sci*. **2022**, *12*, 159–169, https://doi.org/10.7324/JAPS.2022.120418.
27. Edache, E.I.; Ugbe, F.A.; Dawi, H.A.; Adedayo, A.; Umar, A. Mechanism of action of substituted peramivir phosphonate derivatives as potent oseltamivir-resistant influenza A virus using molecular docking, molecular dynamics simulations, and free energies calculations. *Discov. Chem.* **2025**, *2*, 99, https://doi.org/10.1007/s44371-025-00184-1.

28. Dogra, S.; Singh, J.; Koul, B.; Yadav, D. *Artemisia vestita*: A Folk Medicine with Hidden Herbal Fortune. *Molecules* **2023**, *28*, 2788, https://doi.org/10.3390/molecules28062788.
29. Long, A.; Fu, J.; Hu, Y.; Luo, Y. Annphenone from Artemisia vestita Inhibits HepG2 Cell Proliferation. *Asian J. Chem*. **2013**, *25*, 9497–9502, https://doi.org/10.14233/ajchem.2013.15043.
30. Coronado-Aceves, E.W.; Sánchez-Escalante, J.J.; López-Cervantes, J.; Robles-Zepeda, R.E.; Velázquez, C.; Sánchez-Machado, D.I.; Garibay-Escobar, A. Antimycobacterial activity of medicinal plants used by the Mayo people of Sonora, Mexico. *J. Ethnopharmacol.* **2016**, *190*, 106-115, https://doi.org/10.1016/j.jep.2016.05.064.
31. Sah, P.P.T.; Peoples, S.A. The Antitubercular Activity of D-Galacturonic Acid Isonicotinyl Hydrazone*. *J. Am. Pharm. Assoc. (Scientific ed.)* **1953**, *42*, 612-613, https://doi.org/10.1002/jps.3030421009.
32. Uchiyama, T.; Miyase, T.; Ueno, A.; Usmanghani, K. Terpenic glycosides from *Pluchea indica*. *Phytochemistry* **1989**, *28*, 3369-3372, https://doi.org/10.1016/0031-9422(89)80349-8.
33. Alvin, A.; Miller, K.I.; Neilan, B.A. Exploring the potential of endophytes from medicinal plants as sources of antimycobacterial compounds. *Microbiol. Res.* **2014**, *169*, 483-495, https://doi.org/10.1016/j.micres.2013.12.009.
34. Giustarini, D.; Milzani, A.; Dalle-Donne, I.; Rossi, R. How to Increase Cellular Glutathione. *Antioxidants* **2023**, *12*, 1094, https://doi.org/10.3390/antiox12051094.
35. Oboh, H.A.; Muzquiz, M.; Burbano, C.; Cuadrado, C.; Pedrosa, M.M.; Ayet, G.; Osagie, A.U. Anti-nutritional constituents of six underutilized legumes grown in Nigeria. *J. Chromatogr. A* **1998**, *823*, 307-312, https://doi.org/10.1016/S0021-9673(98)00542-1.

Publisher's Note & Disclaimer